

Propyl acetate/butyronitrile mixture is ideally suited for investigating the effect of dielectric stabilization on (photo)chemical reactions

Supporting Information

Pragya Verma, Arnulf Rosspeintner, and Tatu Kumpulainen*

Department of Physical Chemistry, Sciences II, University of Geneva, 30, Quai Ernest Ansermet, 1211 Geneva, Switzerland

E-mail: tatu.kumpulainen@unige.ch

Contents

S1 Physical characterization of PA/BuCN mixture	S3
S1.1 Refractive index	S3
S1.2 Dielectric constant	S3
S1.3 Dynamic viscosity	S4
S1.4 Relation between Δf and w_{PA}	S4
S2 Steady-state solvatochromism	S5
S2.1 Solvatochromism of B30	S5
S2.2 Solvatochromism of C153	S6
S2.3 Solvatochromism of C152A	S7
S2.4 Widths of the absorption and emission bands of coumarins	S8
S3 Estimation of the time-zero emission spectra	S8
S4 Solvation dynamics	S10
S4.1 Solvation dynamics of C153	S10
S4.2 Solvation dynamics of C152A	S12
S5 Rotational diffusion coefficients	S14
S6 Translational diffusion coefficients	S15
S6.1 ^{19}F -DOSY NMR data analysis	S16
S7 Ground-state association and deprotonation constants	S18
S7.1 C_4 -dHONI upon addition of NMI in PA/BuCN mixtures	S20
S7.2 C_4 -dHONI and DBU	S26
References	S31

S1 Physical characterization of PA/BuCN mixture

S1.1 Refractive index

Refractive indices, n_D , were measured using a temperature controlled Abbe refractometer from Atago (model 1T). The refractive indices, presented in Figure S1, are independent of the composition in the solvent mixtures with a mean value of $n_D = 1.3845$.

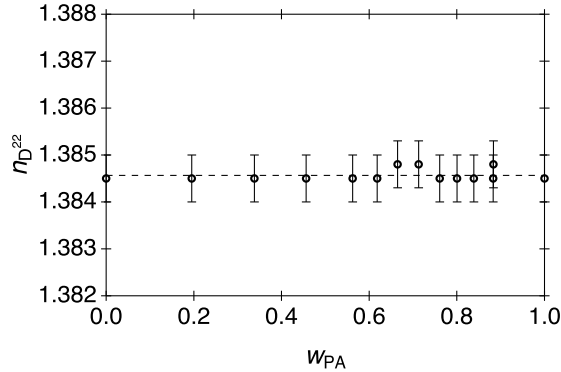


Figure S1: Experimentally determined refractive indices, n_D , as a function of the weight fraction of PA in the PA/BuCN mixtures at 295.2 K.

S1.2 Dielectric constant

Dielectric constants, ϵ_r , were measured using a home-built LC circuit, similar to that discussed in detail in ref. 1, operating at approximately 400 kHz. The experimentally determined dielectric constants, presented in Figure S2, vary linearly with the weight fraction of the PA according to eq. (1) of the main text.

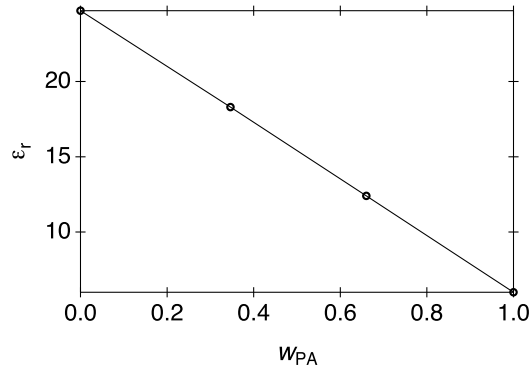


Figure S2: Experimentally determined dielectric constant, ϵ_r , as a function of the weight fraction of PA in the PA/BuCN mixtures at 295.2 K.

S1.3 Dynamic viscosity

The kinematic viscosities, ν , of the mixtures were determined using a thermostatically controlled capillary Ubbelohde viscosimeter (Schott). The dynamic viscosities were calculated from the measured kinematic viscosities according to:

$$\eta = K\bar{t}\rho \quad (\text{S1})$$

where $\nu = K\bar{t}$ is the kinematic viscosity, K the capillary instrument constant, \bar{t} the mean passage time of the liquid and ρ the density of the solvent. Densities of the mixtures were approximated as:

$$\rho_{\text{mix}} = \frac{(m_1 + m_2)\rho_1\rho_2}{m_1\rho_2 + m_2\rho_1} \quad (\text{S2})$$

where ρ_i and m_i are the densities and total masses of the neat solvents in the mixture.

The dynamic viscosities, presented in Figure S3, are independent of the composition of the solvent mixtures with a mean value of $\eta = 0.581$ cP.

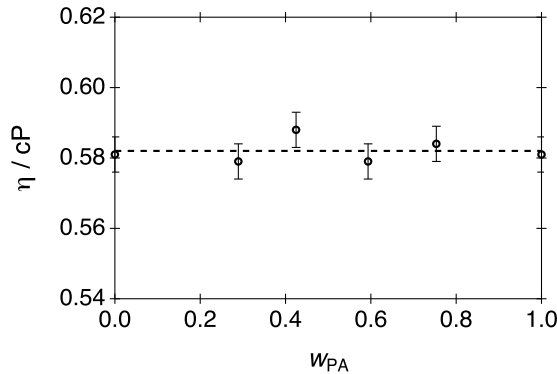


Figure S3: Experimentally determined dynamic viscosities, η , as a function of the weight fraction of PA in the PA/BuCN mixtures at 295.2 K.

S1.4 Relation between Δf and w_{PA}

Although ϵ_r varies linearly with the weight fractions of the solvents, Δf shows nonlinear behavior. Substituting ϵ_r , eq. (1), into eq. (5) of the main text and rearranging yields:

$$\Delta f = \frac{w_{\text{PA}}(\epsilon_r(\text{PA}) - \epsilon_r(\text{BuCN})) + \epsilon_r(\text{BuCN}) - 1}{w_{\text{PA}}(\epsilon_r(\text{PA}) - \epsilon_r(\text{BuCN})) + \epsilon_r(\text{BuCN}) + 1/2} - \frac{2(n^2 - 1)}{2n^2 + 1} \quad (\text{S3})$$

which can be simplified by substituting $\epsilon_r(\text{PA}) - \epsilon_r(\text{BuCN}) = \Delta\epsilon_r$ to :

$$\Delta f = \frac{w_{\text{PA}} \cdot \Delta\epsilon_r + \epsilon_r(\text{BuCN}) - 1}{w_{\text{PA}} \cdot \Delta\epsilon_r + \epsilon_r(\text{BuCN}) + 1/2} - \frac{n^2 - 1}{n^2 + 1/2} \quad (\text{S4})$$

Relation between Δf and the weight fraction of PA, w_{PA} , is graphically presented in Figure S4. The solvation free energy increases sharply upon small additions of BuCN but the changes become gradually more modest at higher BuCN fractions.

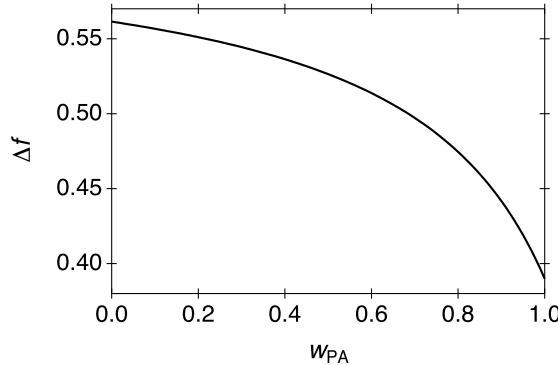


Figure S4: Δf as a function of w_{PA} .

S2 Steady-state solvatochromism

S2.1 Solvatochromism of B30

$E_{\text{T}}(30)$ values, presented in Table S1, were calculated according to eq. (4) of the main text where the B30 absorption band maxima correspond to values obtained by fitting the experimental spectra to a log-normal function.

Table S1: $E_{\text{T}}(30)$ values of the PA/BuCN mixtures

ϵ_r	Δf	FWHM/ 10^3 cm^{-1}	$E_{\text{T}}(30)/\text{kcal mol}^{-1}$	$E_{\text{T}}(30)^a/\text{kcal mol}^{-1}$
6.0	0.3899	3.20	37.54	37.50
6.7	0.4109	3.27	38.40	
7.5	0.4323	3.29	39.04	
8.5	0.4549	3.33	39.73	
10.0	0.4778	3.40	40.34	
11.7	0.4977	3.45	40.84	
14.3	0.5193	3.50	41.40	
18.0	0.5398	3.56	42.01	
24.8	0.5614	3.56	42.63	42.50

^a $E_{\text{T}}(30)$ values from ref. 2.

S2.2 Solvatochromism of C153

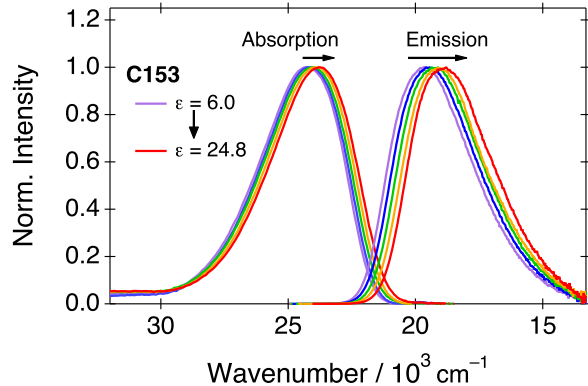


Figure S5: Absorption and emission spectra of C153 in different PA/BuCN mixtures.

Table S2: Frequencies of the absorption and emission band maxima of C153 in PA/BuCN mixtures obtained by fitting the experimental spectra with a log-normal function. The Stokes shifts correspond to a difference in the absorption and emission maxima

Δf	$\tilde{\nu}_{\text{abs}}/10^3 \text{ cm}^{-1}$	$\tilde{\nu}_{\text{flu}}/10^3 \text{ cm}^{-1}$	$\Delta\tilde{\nu}_{\text{Stokes}}/10^3 \text{ cm}^{-1}$
0.3899	24.19	19.68	4.51
0.4129	24.14	19.58	4.57
0.4329	24.10	19.48	4.61
0.4554	24.05	19.38	4.67
0.4756	24.02	19.30	4.72
0.4969	23.93	19.23	4.70
0.5186	23.88	19.15	4.73
0.5401	23.82	19.02	4.80
0.5614	23.76	18.91	4.85

S2.3 Solvatochromism of C152A

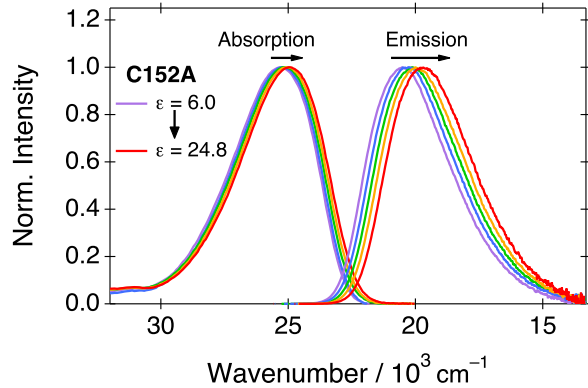


Figure S6: Absorption and emission spectra of C152A in different PA/BuCN mixtures.

Table S3: Frequencies of the absorption and emission band maxima of C152A in PA/BuCN mixtures obtained by fitting the experimental spectra with a log-normal function. The Stokes shifts correspond to a difference in the absorption and emission maxima

Δf	$\tilde{\nu}_{\text{abs}}/10^3 \text{ cm}^{-1}$	$\tilde{\nu}_{\text{flu}}/10^3 \text{ cm}^{-1}$	$\Delta\tilde{\nu}_{\text{Stokes}}/10^3 \text{ cm}^{-1}$
0.3899	25.25	20.57	4.68
0.4129	25.22	20.46	4.76
0.4329	25.18	20.36	4.82
0.4554	25.13	20.27	4.86
0.4756	25.10	20.17	4.93
0.4969	25.04	20.00	5.05
0.5186	25.00	19.98	5.02
0.5401	24.96	19.84	5.12
0.5614	24.92	19.72	5.20

S2.4 Widths of the absorption and emission bands of coumarins

The band frequencies and hence the solvatochromic analyses in wavenumber representation are misleading due to the fact that the intrinsic lineshapes depend on the frequency. It is well known that the mirror image symmetry should hold only in the so-called transition dipole moment (TDM) representation.³ This is evident from the full-width at half maximum (FWHM) values of the absorption and emission spectra. In TDM representation, the widths for absorption and emission are very similar whereas they differ by more than 500 cm⁻¹ in the wavenumber representation. Due to this reason, why we chose to use the TDM representation for the solvatochromic analyses of the coumarins.

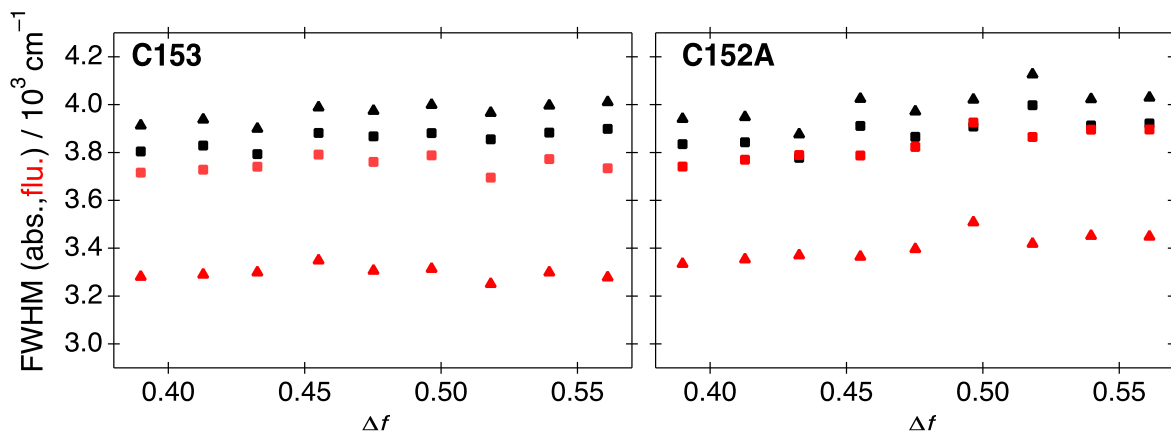


Figure S7: Full-width at half maxima (FWHM) of the absorption and emission bands of C152A and C153 in different PA/BuCN mixtures. The triangles correspond to the values obtained from the spectra in wavenumber representation whereas the squares correspond to the values obtained from the spectra in transition dipole moment (TDM) representation.

S3 Estimation of the time-zero emission spectra

The time-zero emission spectra in PA/BuCN mixtures were estimated with the method described by Maroncelli and coworkers.^{4,5} In brief, absorption and emission spectra of each compound are measured in a nonpolar solvent (2-methylbutane) and used as intrinsic band-shape functions after conversion to the transition dipole moment representation.³ The absorption in polar solvent is fitted with a convolution integral of the intrinsic band-shape function and a Gaussian with two adjustable parameters, the width and the shift of the Gaussian. These parameters represent the broadening and the solvatochromic shift, respectively, due to the polar environment. The parameters of the Gaussian obtained are then used to convolve the intrinsic emission band-shape function to obtain the final time-zero

emission spectrum in the polar solvent. Full details of the method are described in ref. 4. The band shape parameters of the time-zero emission spectra were obtained from fits with the log-normal function. Representative spectra of both coumarins in nonpolar solvent and in neat PA are presented in Figure S8 and all the best-fit parameters are given in Table S4.

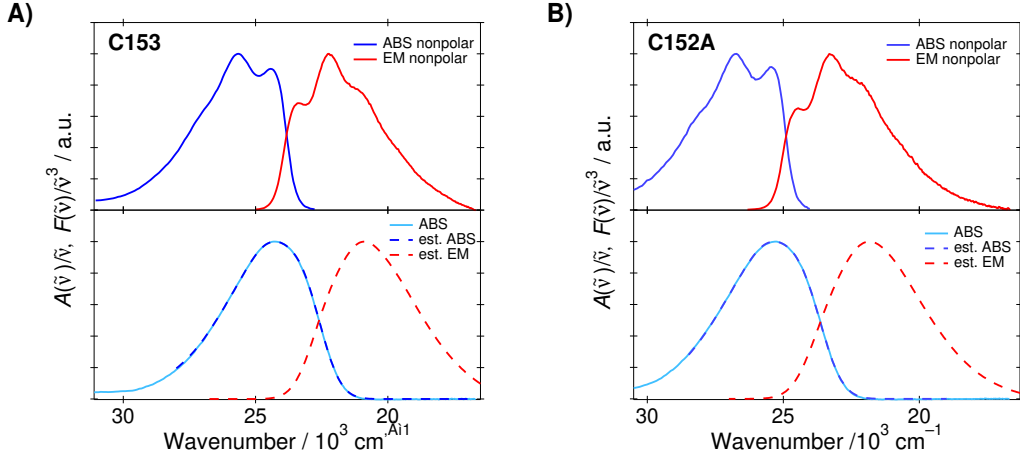


Figure S8: **Top panels:** Absorption (blue) and emission (red) spectra of A) C153 and B) C152A in 2-methylbutane. **Bottom panels:** Measured (blue solid line) and estimated (dashed blue line) absorption spectra together with the estimated (dashed red line) time-zero emission spectra in PA.

Table S4: Parameters of the Gaussian used to estimate the time-zero emission spectra in PA/BuCN mixtures and log-normal best-fit parameters of the estimated $t=0$ spectra. All parameters (except b) are given in 10^3 cm^{-1}

Δf	Gaussian		log-normal		
	shift	FWHM	$\tilde{\nu}_0$	FWHM	b
C153					
0.39	-1.19	1.35	20.87	3.86	-0.26
0.43	-1.29	1.37	20.77	3.87	-0.26
0.48	-1.39	1.47	20.66	3.91	-0.25
0.52	-1.51	1.48	20.54	3.91	-0.25
0.56	-1.64	1.56	20.39	3.95	-0.25
C152A					
0.39	-1.19	1.44	21.83	4.01	-0.27
0.43	-1.27	1.43	21.75	4.01	-0.27
0.48	-1.36	1.55	21.65	4.05	-0.26
0.52	-1.45	1.58	21.56	4.06	-0.25
0.56	-1.55	1.65	21.45	4.09	-0.25

S4 Solvation dynamics

S4.1 Solvation dynamics of C153

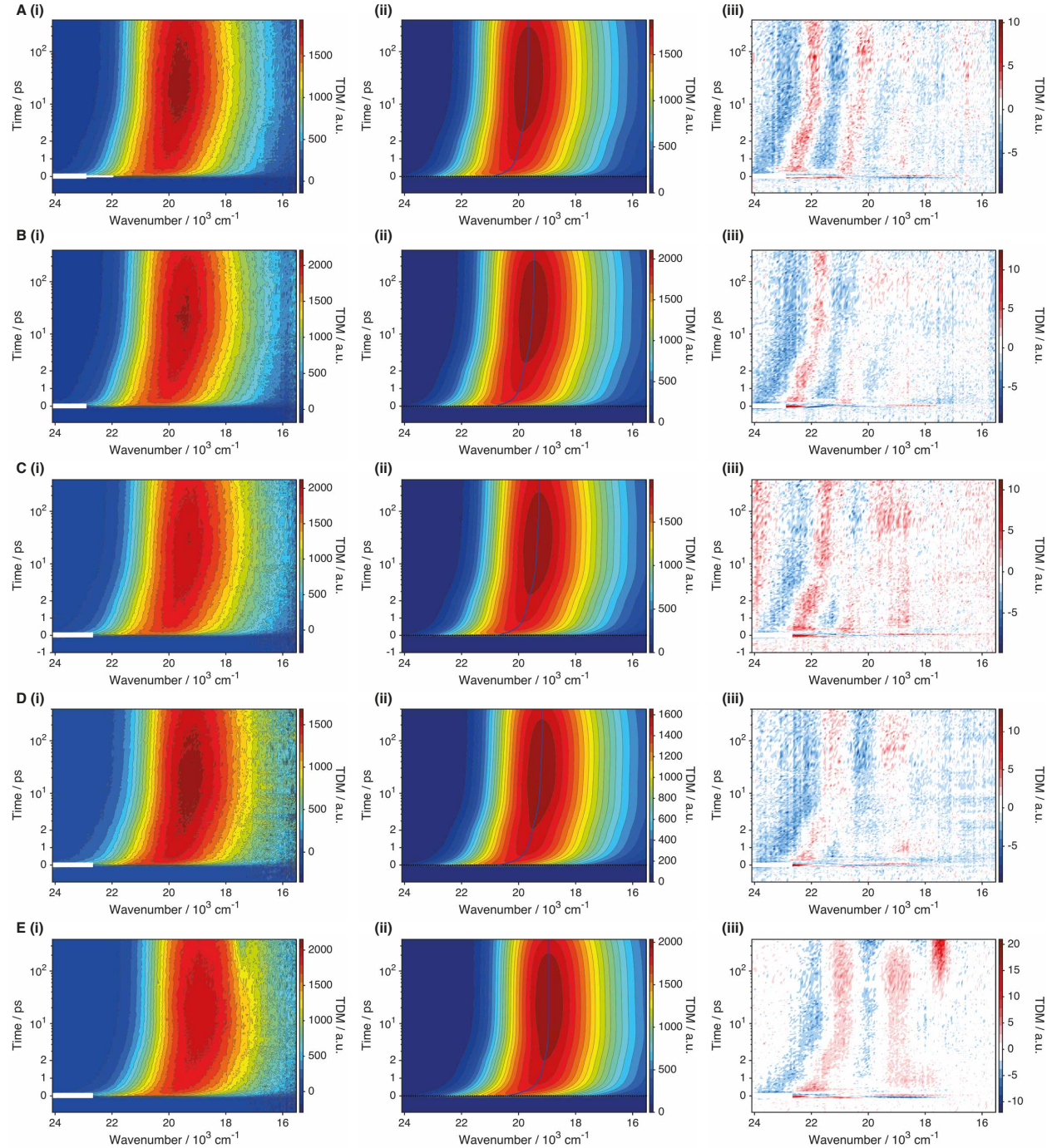


Figure S9: (i) Time-resolved fluorescence of C153 in Pu/BuCN mixtures, (ii) best global fits and (iii) weighted residuals, on a lin-log time axis. The blue lines in the middle panels represents the band maxima. The blank white area is excluded from the fit due to scattering. Dielectric constant increases from A to E corresponding to Δf the values given in Table S5.

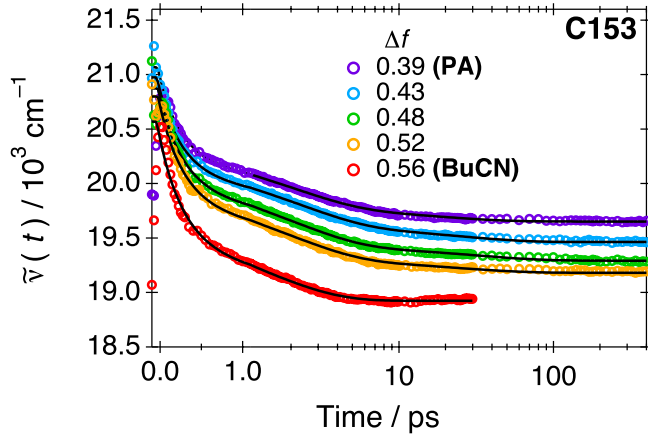


Figure S10: Time-dependent fluorescence band position of C153 in the PA/BuCN mixtures. The solid lines represent the band positions obtained from the global analysis corresponding to two- or three-exponential functions. The best-fit parameters of the exponential functions are given in Table S6. The data in BuCN is fitted only up to 30 ps due to a spectral artifact.

Table S5: Spectral parameters obtained either from the global analysis of the time-resolved (TR) or estimated from the steady-state (SS) fluorescence spectra of C153 in PA/BuCN mixtures^a

Δf	time-zero			relaxed			total shift		
	$\tilde{\nu}_{t=0}^{\text{TR}}$	$\tilde{\nu}_{t=0}^{\text{SS}}$	$\Delta\tilde{\nu}_{t=0}$	$\tilde{\nu}_{t=\infty}^{\text{TR}}$	$\tilde{\nu}_{t=\infty}^{\text{SS}}$	$\Delta\tilde{\nu}_{t=\infty}$	$\Delta\tilde{\nu}_{\text{tot}}^{\text{TR}}$	$\Delta\tilde{\nu}_{\text{tot}}^{\text{SS}}$	$\Delta\Delta\tilde{\nu}_{\text{tot}}$
0.39	21.07	20.87	0.20	19.65	19.68	-0.03	1.42	1.19	0.23
0.43	20.98	20.77	0.20	19.46	19.49	-0.03	1.51	1.28	0.23
0.48	20.87	20.66	0.22	19.29	19.30	-0.01	1.58	1.36	0.23
0.52	20.80	20.54	0.26	19.18	19.12	0.06	1.62	1.42	0.20
0.56	20.57	20.39	0.18	18.92	18.91	0.01	1.65	1.48	0.16

^aAll spectral parameters are given in 10^3 cm^{-1} . $\tilde{\nu}_{t=0}^{\text{SS}}$ and $\tilde{\nu}_{t=\infty}^{\text{SS}}$ correspond to the frequencies of the estimated time-zero and the relaxed steady-state fluorescence band maxima and $\Delta\tilde{\nu}_{\text{tot}}^{\text{SS}}$ corresponds to the total shift. $\tilde{\nu}_{t=0}^{\text{TR}}, \tilde{\nu}_{t=\infty}^{\text{TR}}$, and $\Delta\tilde{\nu}_{\text{tot}}^{\text{TR}}$ are the corresponding values obtained from the global analysis of the time resolved fluorescence spectra. $\Delta\Delta\tilde{\nu}_{\text{tot}}$ is the difference between the total shifts.

Table S6: Amplitudes (%) and lifetimes (ps) of solvation dynamics of C153 in PA/BuCN mixtures obtained from the global analysis

Δf	α_1	τ_1	α_2	τ_2	α_3	τ_3	$\langle \tau_{\text{solv}} \rangle^a$	χ^2
0.39	0.54	0.2	0.37	2.2	0.09	18.4	2.5	2.00
0.43	0.53	0.3	0.38	2.4	0.10	24.7	3.4	1.88
0.48	0.53	0.3	0.39	2.2	0.08	31.7	3.7	1.82
0.52	0.55	0.3	0.37	2.1	0.07	24.2	2.7	1.94
0.56	0.61	0.3	0.39	1.6	—	—	0.8	2.69

^aThe mean solvation time was calculated according to $\langle \tau_{\text{solv}} \rangle = \Sigma \alpha_i \tau_i$ where the amplitudes, α_i , are normalized.

S4.2 Solvation dynamics of C152A

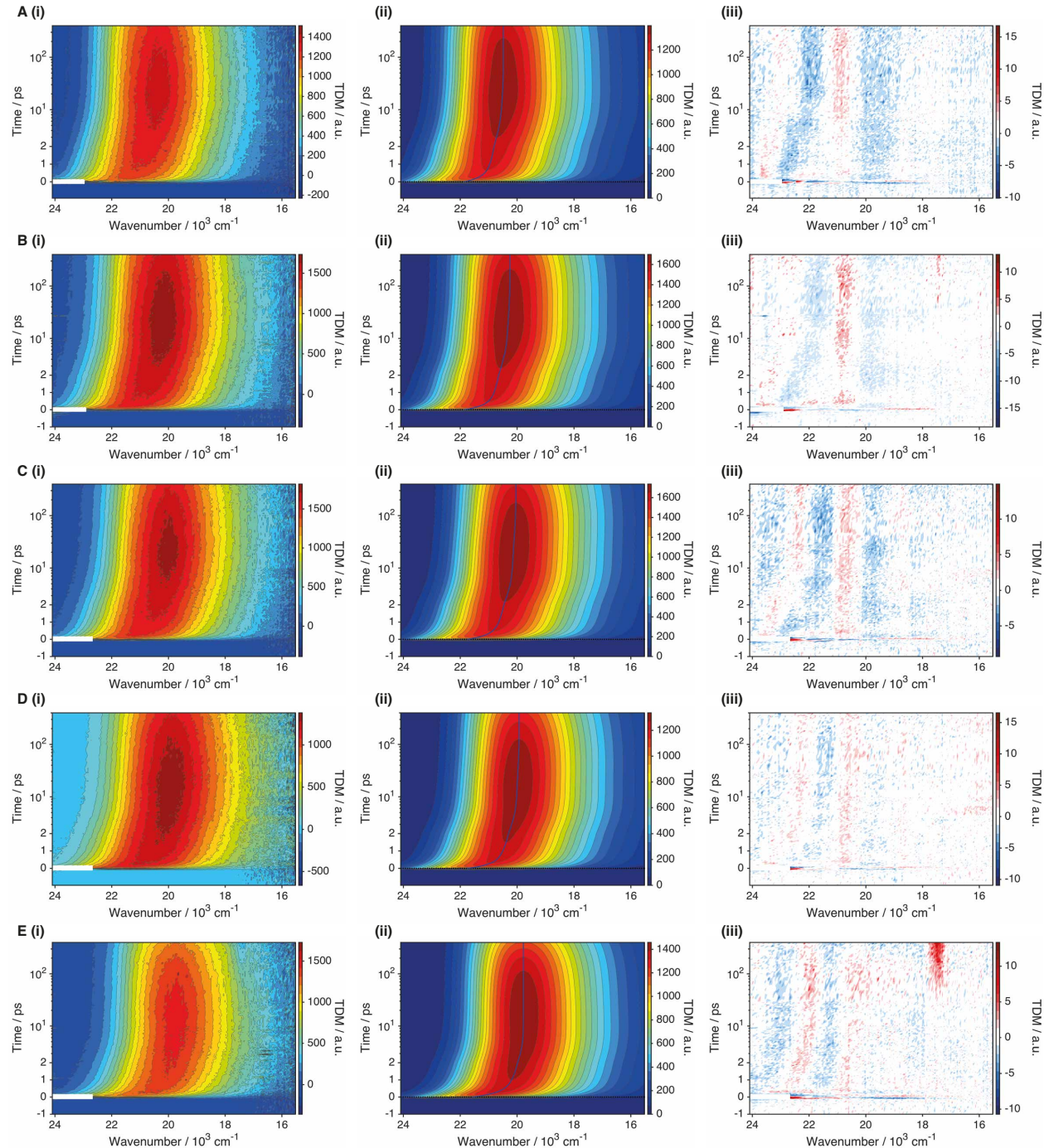


Figure S11: (i) Time-resolved fluorescence of C152A in Pu/BuCN mixtures, (ii) best global fits and (iii) weighted residuals, on a lin-log time axis. The blue lines in the middle panels represents the band maxima. The blank white area is excluded from the fit due to scattering. Dielectric constant increases from A to E corresponding to Δf the values given in Table S7.

Table S7: Spectral parameters obtained either from the global analysis of the time-resolved (TR) or estimated from the steady-state fluorescence spectra of C152A in PA/BuCN mixtures^a

Δf	time-zero			relaxed			total shift		
	$\tilde{\nu}_{t=0}^{\text{TR}}$	$\tilde{\nu}_{t=0}^{\text{SS}}$	$\Delta\tilde{\nu}_{t=0}$	$\tilde{\nu}_{t=\infty}^{\text{TR}}$	$\tilde{\nu}_{t=\infty}^{\text{SS}}$	$\Delta\tilde{\nu}_{t=\infty}$	$\Delta\tilde{\nu}_{\text{tot}}^{\text{TR}}$	$\Delta\tilde{\nu}_{\text{tot}}^{\text{SS}}$	$\Delta\Delta\tilde{\nu}_{\text{tot}}$
0.39	21.99	21.83	0.15	20.48	20.57	-0.09	1.50	1.26	0.24
0.43	21.98	21.75	0.22	20.25	20.36	-0.32	1.72	1.39	0.33
0.48	21.92	21.65	0.27	20.04	20.15	-0.53	1.87	1.50	0.37
0.52	21.92	21.56	0.36	19.93	19.94	-0.64	1.99	1.62	0.37
0.56	21.80	21.45	0.35	19.78	19.72	-0.79	2.02	1.72	0.30

^aAll spectral parameters are given in 10^3 cm^{-1} . $\tilde{\nu}_{t=0}^{\text{SS}}$ and $\tilde{\nu}_{t=\infty}^{\text{SS}}$ correspond to the frequencies of the estimated time-zero and the relaxed steady-state fluorescence band maxima and $\Delta\tilde{\nu}_{\text{tot}}^{\text{SS}}$ corresponds to the total shift. $\tilde{\nu}_{t=0}^{\text{TR}}, \tilde{\nu}_{t=\infty}^{\text{TR}}$, and $\Delta\tilde{\nu}_{\text{tot}}^{\text{TR}}$ are the corresponding values obtained from the global analysis of the time resolved fluorescence spectra. $\Delta\Delta\tilde{\nu}_{\text{tot}}$ is the difference between the total shifts.

Table S8: Amplitudes (%) and lifetimes (ps) of solvation dynamics of C152A in PA/BuCN mixtures obtained from the global analysis

Δf	α_1	τ_1	α_2	τ_2	α_3	τ_3	$\langle\tau_{\text{solv.}}\rangle^a$	χ^2
0.39	0.54	0.3	0.36	2.1	0.09	13.3	2.1	1.64
0.43	0.55	0.2	0.37	2.3	0.08	25.8	3.1	1.83
0.48	0.53	0.2	0.39	2.1	0.08	40.4	4.2	1.61
0.52	0.55	0.2	0.40	1.9	0.06	30.7	2.7	1.37
0.56	0.62	0.2	0.38	1.6	0.00	0.0	0.7	1.75

^aThe mean solvation time was calculated according to $\langle\tau_{\text{solv.}}\rangle = \Sigma\alpha_i\tau_i$ where the amplitudes, α_i , are normalized.

S5 Rotational diffusion coefficients

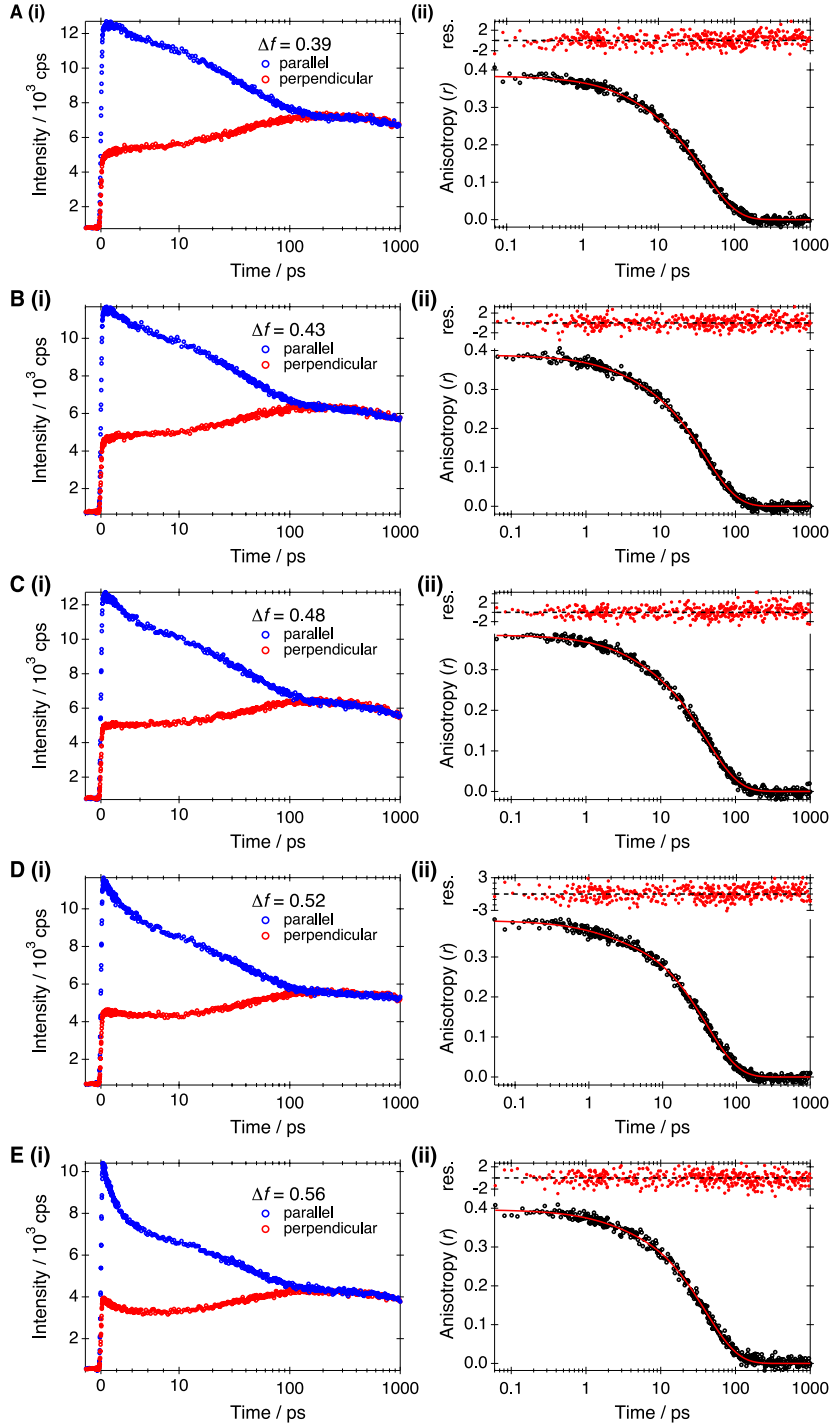


Figure S12: (i) Fluorescence decays of C153 in PA/BuCN mixtures measured at parallel (blue) and perpendicular (red) polarizations of the pump pulse. (ii) Fluorescence anisotropy decays together with bi-exponential fits. The weighted residuals are shown in the top panels. The best-fit parameters are given in Table S9. Dielectric constant increases from A to E. Excitation and monitoring wavelengths were 400 nm and 500 nm, respectively.

Table S9: Fluorescence anisotropy decay parameters of C153 in PA/BuCN mixtures obtained from fits with a bi-exponential function

Δf	r_0	α_1	τ_1/ps	α_2	τ_2/ps	$\langle \tau_{\text{rot.}} \rangle/\text{ps}^a$	χ^2
0.3899	0.38	0.11	3.8	0.89	40.3	36.4 ± 0.8	1.20
0.4332	0.39	0.09	2.8	0.91	39.2	35.8 ± 0.6	1.06
0.4758	0.39	0.10	3.7	0.90	41.2	37.5 ± 0.8	1.22
0.5187	0.39	0.09	1.4	0.91	39.4	36.1 ± 0.5	1.18
0.5614	0.40	0.08	2.0	0.92	39.8	36.9 ± 0.6	1.09

^aThe mean rotational time was calculated according to $\langle \tau_{\text{rot.}} \rangle = \sum \alpha_i \tau_i$ where the amplitudes, α_i , are normalized.

The raw decays were fitted with a multi-exponential function convolved with a Gaussian-simulated instrument response function to obtain reasonable estimations for the time zero of each decay and the decays were shifted to match the time-zero values. Due to significant background counts before time zero, the anisotropy were constructed from the fluorescence decays according to the following relation:

$$r(t) = \frac{[I(t)_{||} - bg_{||}] - [I(t)_{\perp} - bg_{\perp}]}{[I(t)_{||} - bg_{||}] + 2[I(t)_{\perp} - bg_{\perp}]} \quad (\text{S5})$$

where $I(t)_{||}$, $I(t)_{\perp}$ are parallel and perpendicular intensity, respectively and bg_i is corresponding mean intensity before time zero. The final uncertainties in $r(t)$ were calculated by error propagation using the following relation:

$$\Delta r = \sqrt{\left(\frac{\partial r}{\partial I_{||}} \Delta I_{||} \right)^2 + \left(\frac{\partial r}{\partial I_{\perp}} \Delta I_{\perp} \right)^2} \quad (\text{S6})$$

where $\Delta I_{||} = \sqrt{I_{||}}$ and $\Delta I_{\perp} = \sqrt{I_{\perp}}$ following Poisson counting statistics and $\Delta bg = 0$. The anisotropy decays were analyzed with a bi-exponential function from $t > 50$ fs. The fits were weighted with the above uncertainties to obtain meaningful χ^2_r values.

S6 Translational diffusion coefficients

The NMR experiments were recorded at a temperature of 298 K on a Bruker Avance III HD-NanoBay 300 MHz spectrometer ^1H NMR Larmor frequency with a 5-mm BB(F)-H-D probe equipped with a z-gradient coil of maximum nominal gradient strength of 50.5 G cm^{-1} .

The ^{19}F -DOSY experiments were carried out without locking. The pulse program was *dstegp3s*. The diffusion time was 30 ms and the gradient pulse 3.0 ms. Duration of the spoiling gradient was 0.6 ms. The top amplitude of the diffusion gradients ranged from 2.5

to 42.9 G/cm (5-85% of the maximal power) in 16 linear steps. The spectral windows were set to 200 ppm and 10 ppm in F2 and F1 and the spectra acquired with 64 k and 16 points, respectively. The recovery delay was set to 2.0 s. Total experimental time was 22 min with the number of scans $ns = 32$ and the dummy scans set to 4.

The diffusion coefficient were extracted from the ^{19}F -DOSY data using the built-in analysis routines in MNova (Mestrelab Research) and TopSpin (Bruker) softwares. The values obtained from two analyses differed slightly and the reported values correspond to the mean values from the two analyses and the errors represent the corresponding standard deviations.

S6.1 ^{19}F -DOSY NMR data analysis

The integrated intensities of the NMR peaks were fitted with a three-parameter exponential fit:

$$Y = B + F \times \exp(-XG) \quad (\text{S7})$$

where B is the baseline offset, F the initial amplitude and G the diffusion coefficient in cm^2/s . The intensity decays together with the exponential best-fits are presented in Figure S13. The diffusion constants obtained from each of the analyses (Mnova and TopSpin) together with the mean values are given in Table S10.

Table S10: Translational diffusion coefficients of C153 in PA/BuCN mixtures. All parameters are given in $10^{-9} \text{ m}^2\text{s}^{-1}$

Δf	D_{TopSpin}	D_{Mnova}	$\langle D \rangle$	σ
0.3899	1.15	0.96	1.05	0.09
0.4340	1.15	0.99	1.07	0.08
0.4778	1.14	0.99	1.06	0.08
0.5185	1.13	0.94	1.03	0.09
0.5614	1.12	0.95	1.03	0.09

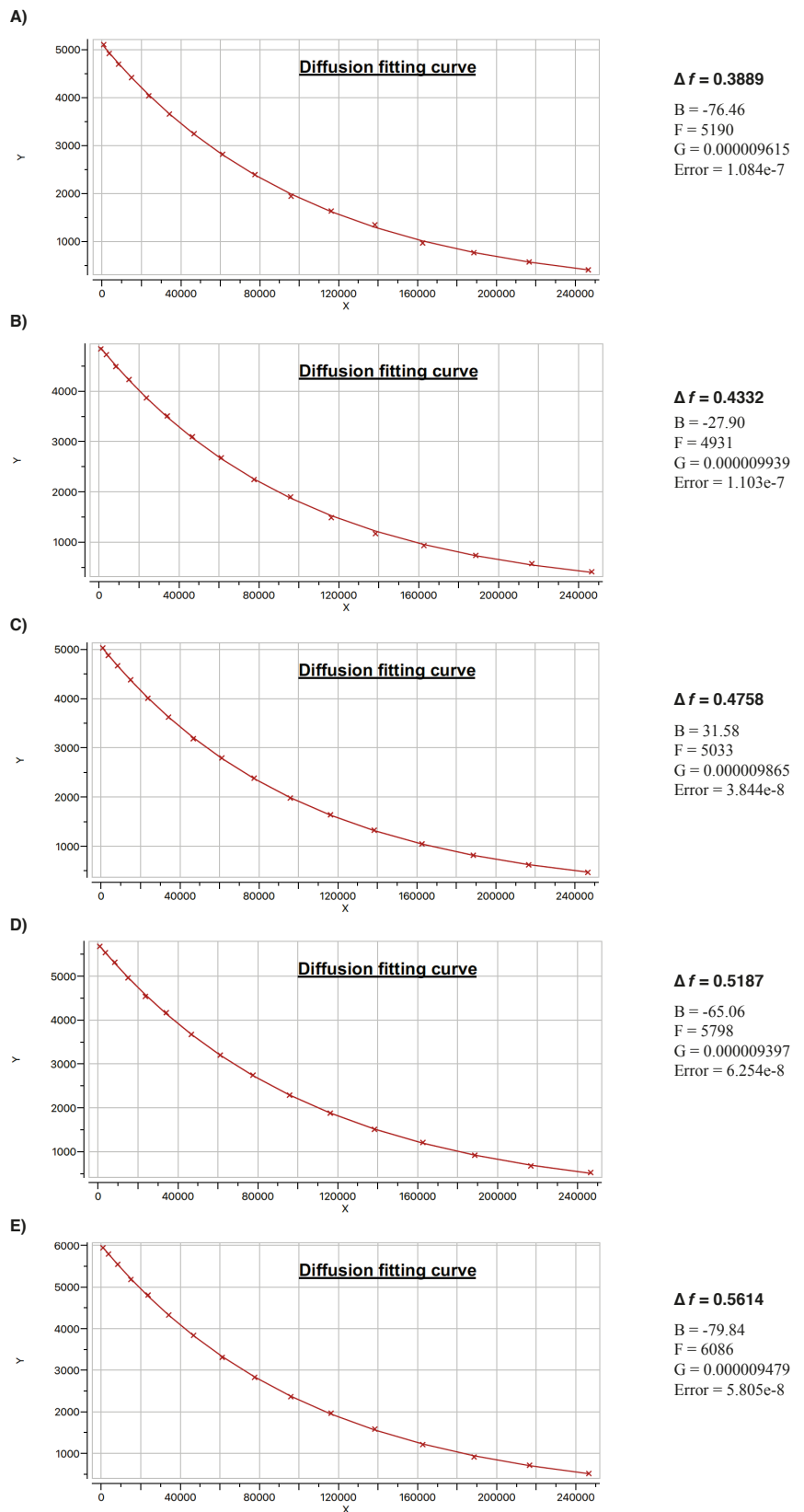
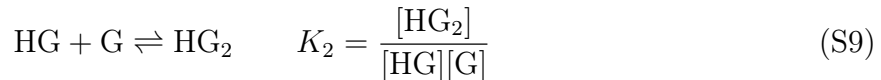
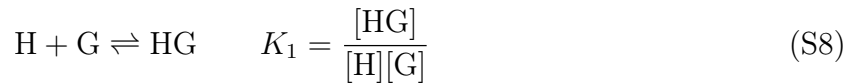


Figure S13: Integrals of the ^{19}F -DOSY NMR data of C153 in PA/BuCN mixtures with increasing Δf from A to E together with the exponential fits using the Mnova software.

S7 Ground-state association and deprotonation constants

The derivation of the fit functions for 1:2 host(H)-guest(G) association is heavily adopted from the approach presented in ref. 6. Only the key equations are reproduced here but all intermediate equations are given in refs. 6 and 7.

The two equilibrium reactions and corresponding association constants are:



where K_1 and K_2 are the association constant for the formation of 1:1 and 1:2 complexes, respectively, and $[X]$ corresponds to the concentration of the free host (H), free guest (G), 1:1 complex (HG) or 1:2 complex (HG_2). The total concentration of each species can be derived from the stoichiometry according to:

$$[H]_0 = [H] + [HG] + [HG_2] \quad (S10)$$

$$[G]_0 = [G] + [HG] + 2[HG_2] \quad (S11)$$

Using the above relations, expressions for $[H]$, $[HG]$, and $[HG_2]$ can be derived in terms of a single concentration dependent unknown, $[G]$, and the constants, $[H]_0$ K_1 and K_2 . Similarly, $[G]_0$ can be expressed as:

$$[G]_0 = [G] + \frac{K_1[G] + 2K_1K_2[G]^2}{1 + K_1[G] + K_1K_2[G]^2} [H]_0 \quad (S12)$$

The above equation can be rearranged to solve for $[G]$ resulting a cubic equation. The correct root can be estimated analytically (smallest positive real number) or numerically using the Newton-Raphson method, for example. Once $[G]$ has been solved, all the concentrations can be calculated analytically.

With an expression for one of the concentrations in hand, we need to derive a relationship between the absorption and the guest concentration, $[G]$. We start by expressing the total absorbance as a function of molar fractions, f , and assume that the free guest does not absorb at the monitoring wavelength (this can be experimentally achieved by selecting the monitoring wavelength higher than the guest absorption or by subtracting the guest

concentration from the sample concentration, we use the latter).

$$A(\lambda) = A_H(\lambda)f_H + A_{HG}(\lambda)f_{HG} + A_{HG_2}(\lambda)f_{HG_2} \quad (\text{S13})$$

where $A(\lambda)_i$ is the absorption of each species. Using $f_X = [\text{X}]/[\text{H}]_0$ and substituting the concentrations into eq. (S13) we obtain the final expression that is used in the non-linear least squares fitting.

$$A(\lambda) = \frac{A_H(\lambda) + A_{HG}(\lambda)K_1[G] + A_{HG_2}(\lambda)K_1K_2[G]^2}{1 + K_1[G] + K_1K_2[G]^2} \quad (\text{S14})$$

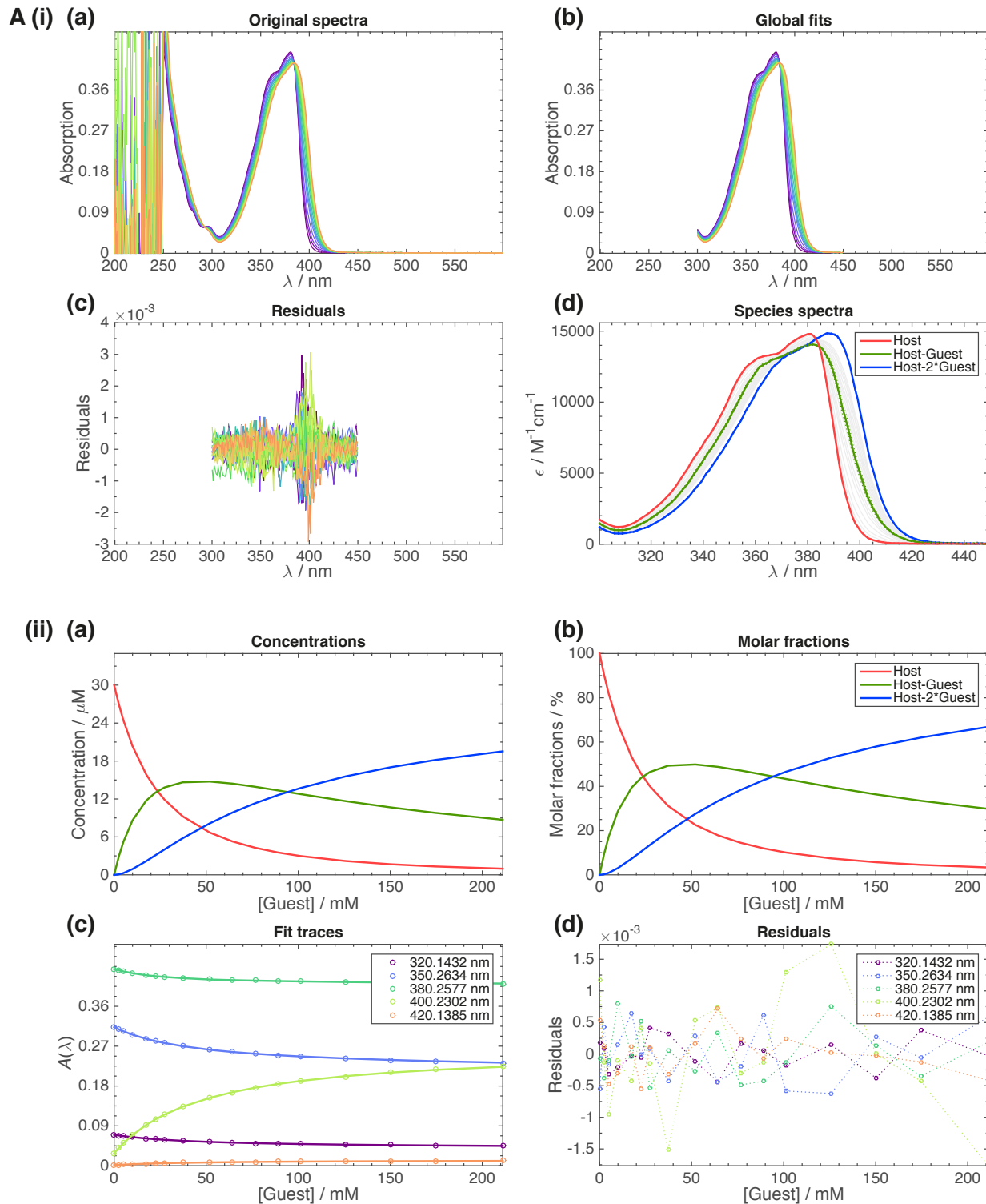
The fitting parameters are the absorptions of the host, $A_H(\lambda)$, 1:1 complex, $A_{HG}(\lambda)$, and 1:2 complex, $A_{HG_2}(\lambda)$, corresponding to the total concentration of the host, $[\text{H}]_0$, and the association constants, K_1 and K_2 . The total host and guest concentrations are known from the experimental conditions. An experimental titration curve is obtained by plotting the absorption as a function of the total guest concentration. The complete spectra of all the species can be obtained by fitting the absorption spectra over a broad wavelength range.

We have previously demonstrated that weak bases form neutral hydrogen-bonded complexes with the C₄-dHONI photoacid. Moreover, the association shows non-cooperative behavior i.e. $K_1 = 4K_2$. This was implicitly assumed in the analysis to reduce the number of variables. Strong bases, on the other hand, will at least partially deprotonate a single hydroxyl group followed by an association of a second base to the remaining free hydroxyl group.⁷ Moreover, the association is shows strong negative cooperativity i.e. $K_1 > 4K_2$. Therefore, the first association constant, K_1 represents a deprotonation constant and is expected to respond strongly to the polarity of the solvent mixture.

Representative absorption spectra of C₄-dHONI upon addition of NMI and DBU in a PA/BuCN solvent mixture with $\Delta f = 0.48$ are presented in Figure 5 of main text. The spectra and fit results in all mixtures are given below. The top parts (i) of the figures present (a) the experimental absorption spectra, (b) global best-fits, (c) residuals, and (d) the species spectra in the units of molar absorptivity ($\text{M}^{-1}\text{cm}^{-1}$). The bottom parts (ii) present (a) the concentrations the species, (b) molar fractions, f_X , (c) example titration traces and fits at selected wavelengths, and (d) residuals at the same wavelengths. The association constants with NMI are presented in Table S11 and the depronation/association constants with DBU in Table S12.

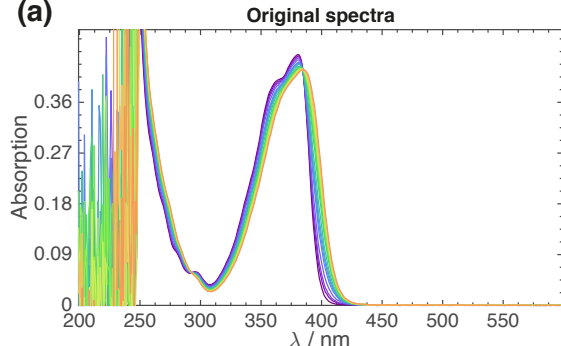
S7.1 C₄-dHONI upon addition of NMI in PA/BuCN mixtures

$$\Delta f = 0.3899$$

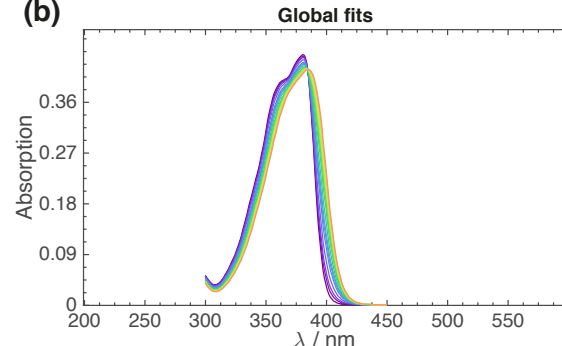


$$\Delta f = 0.4328$$

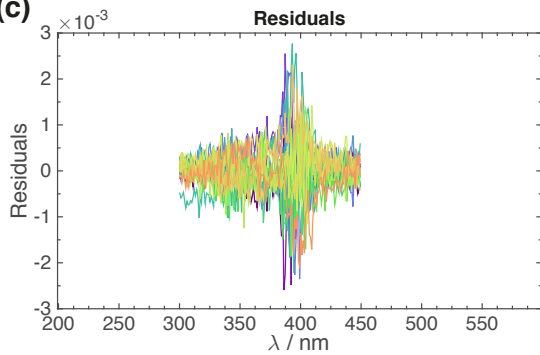
B (i) (a)



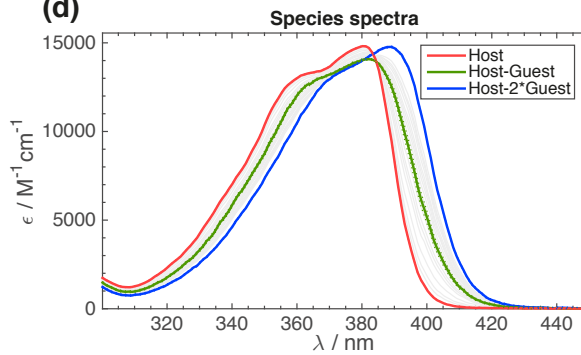
(b)



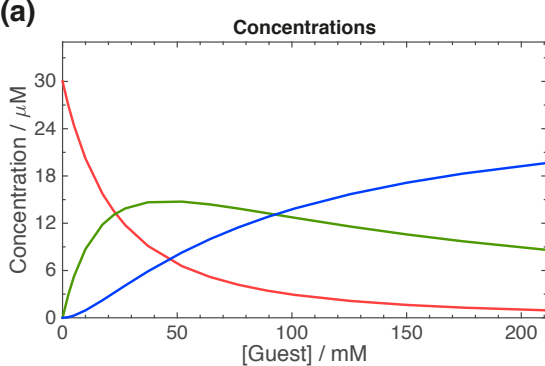
(c)



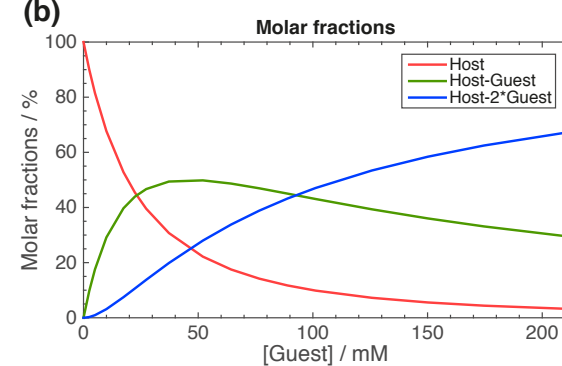
(d)



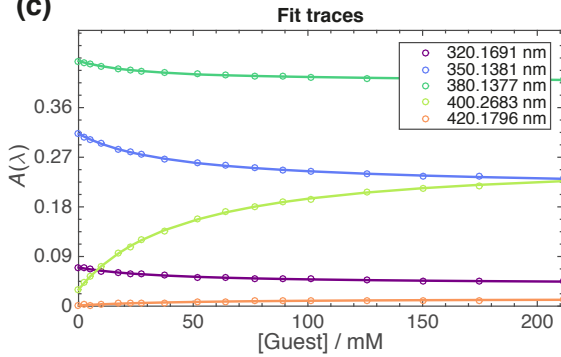
(ii) (a)



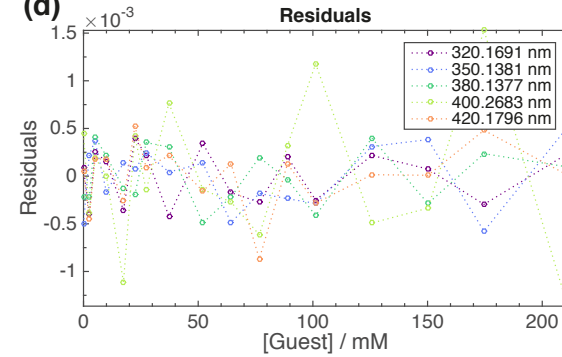
(b)



(c)

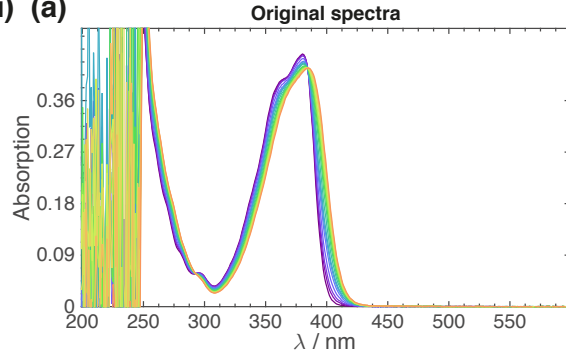


(d)

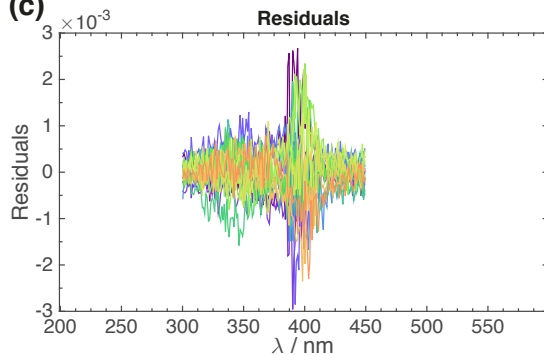


$$\Delta f = 0.4756$$

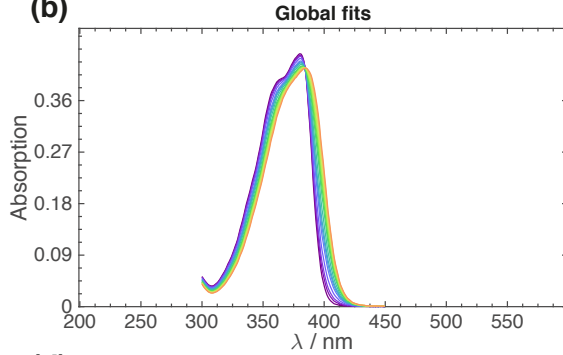
C (i) (a)



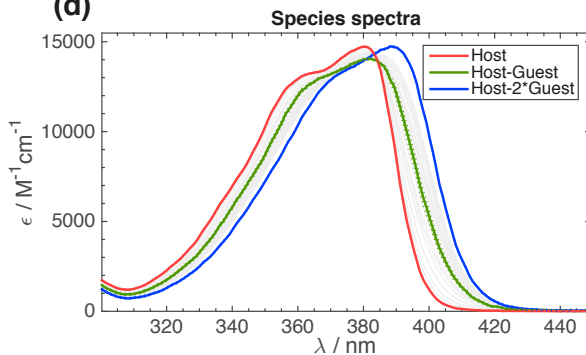
(c)



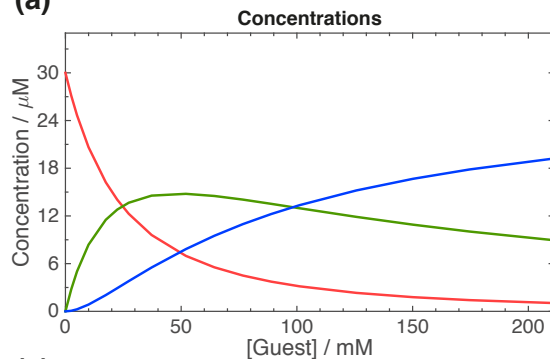
(b)



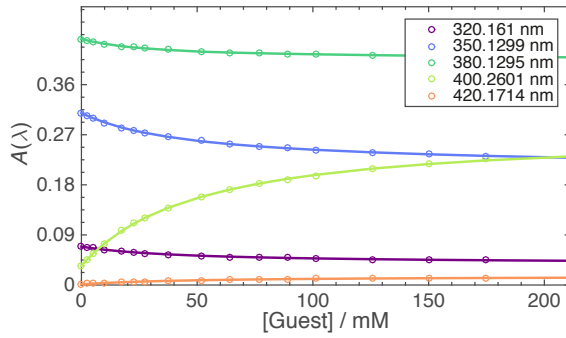
(d)



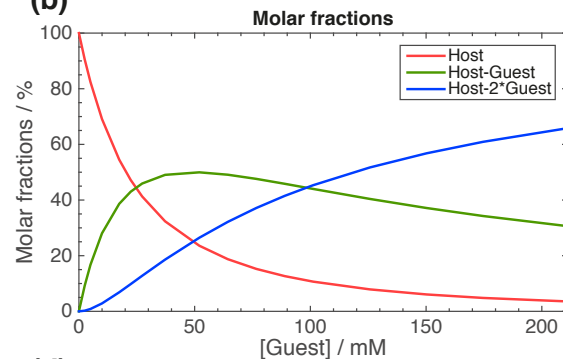
(ii) (a)



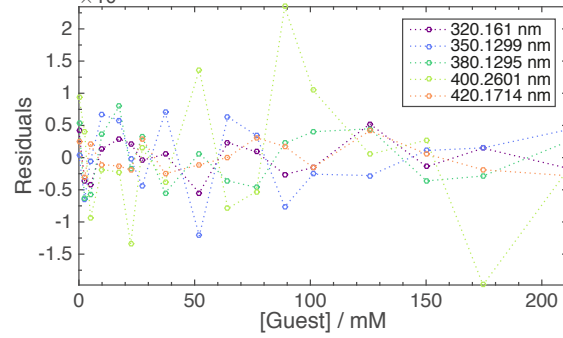
(c)



(b)

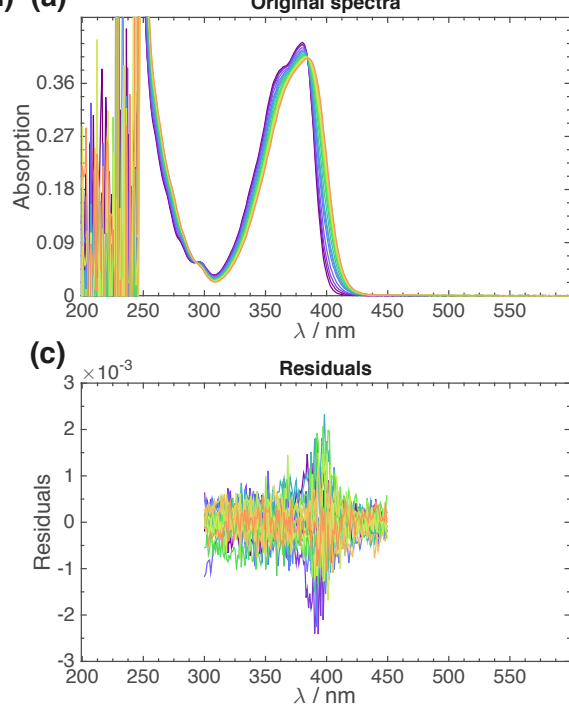


(d)

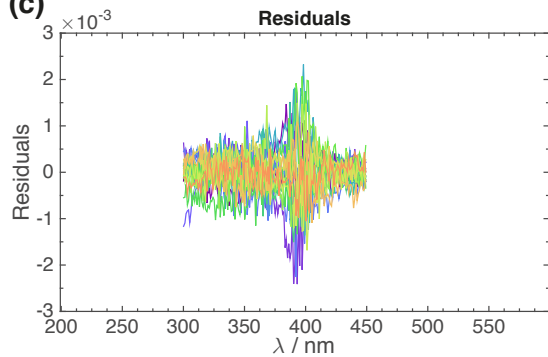


$$\Delta f = 0.5187$$

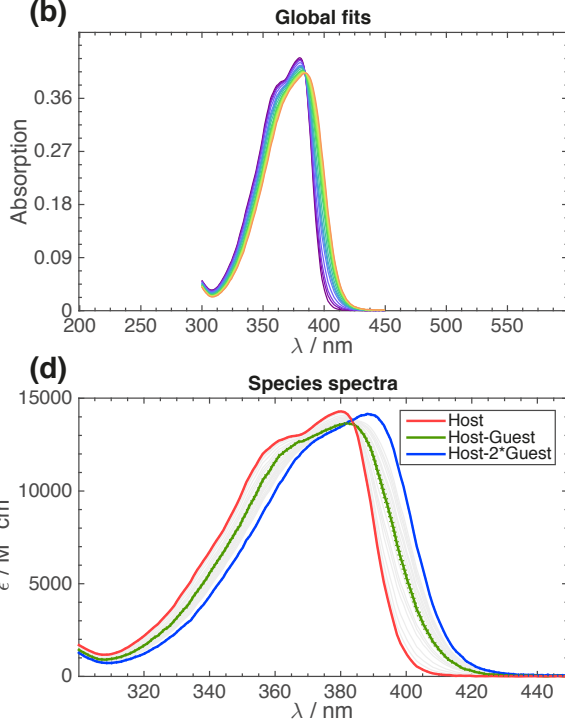
D (i) (a)



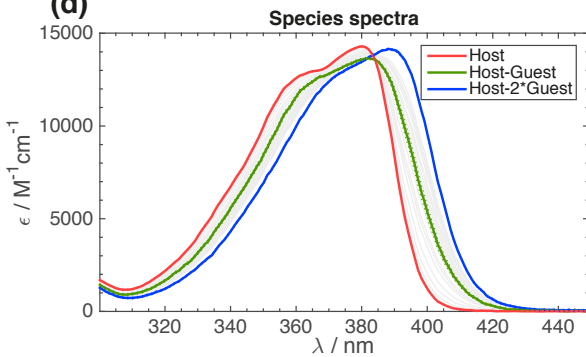
(c)



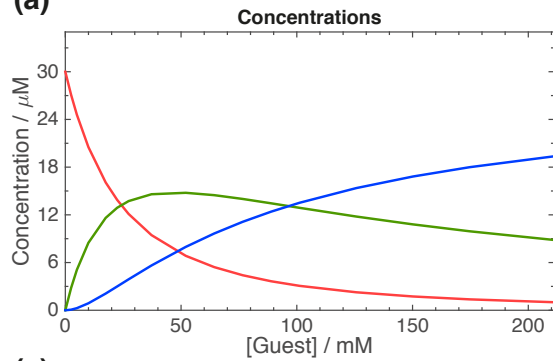
(b)



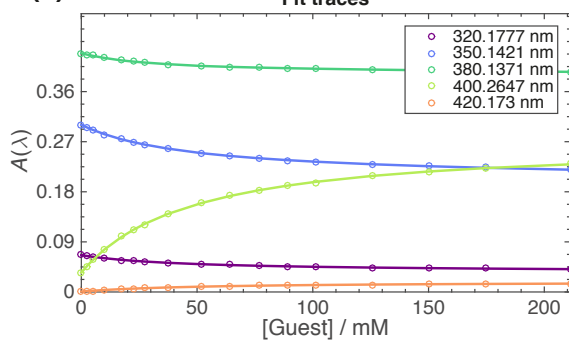
(d)



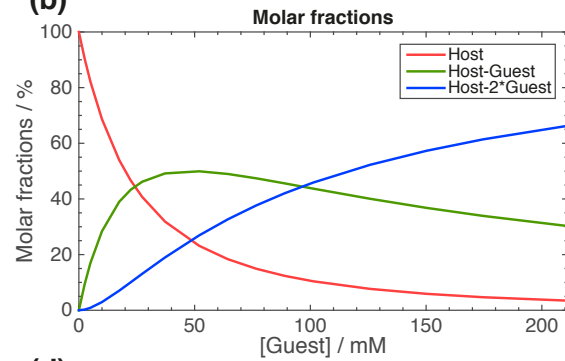
(ii) (a)



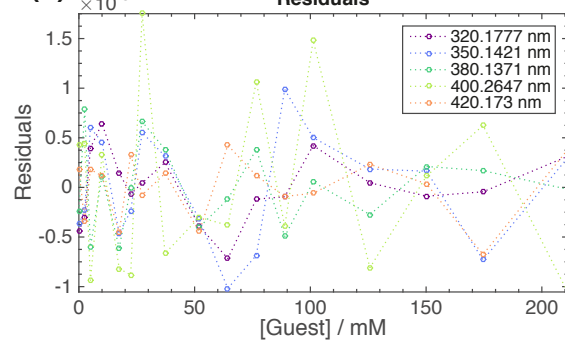
(c)



(b)

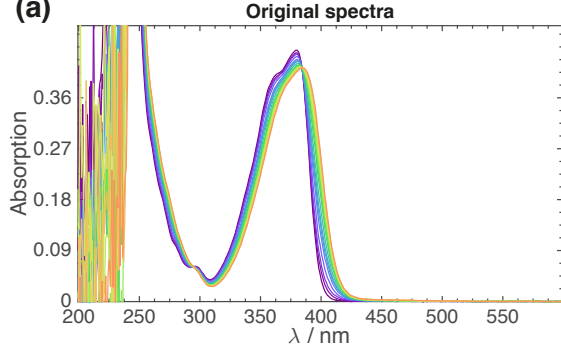


(d)

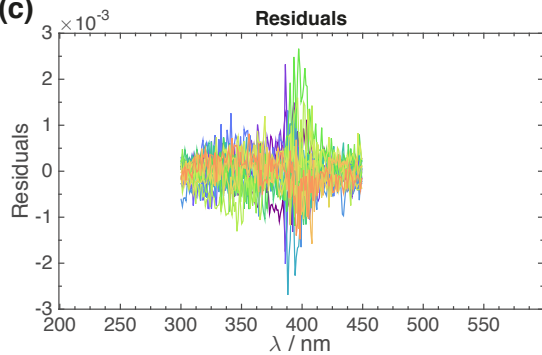


$$\Delta f = 0.5614$$

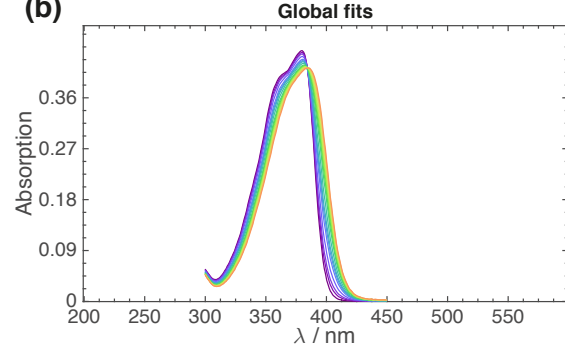
E (i) (a)



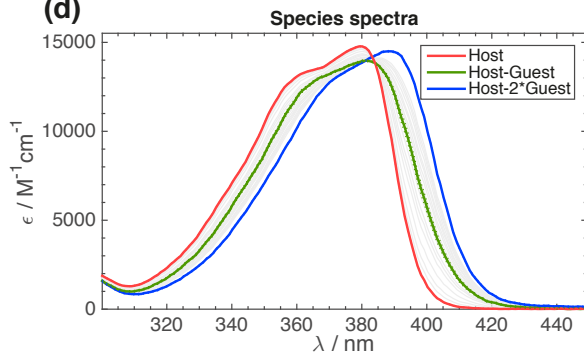
(c)



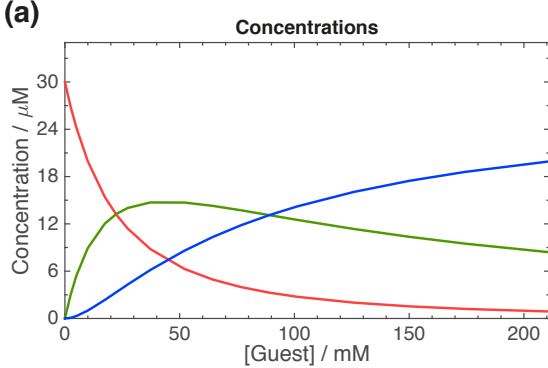
(b)



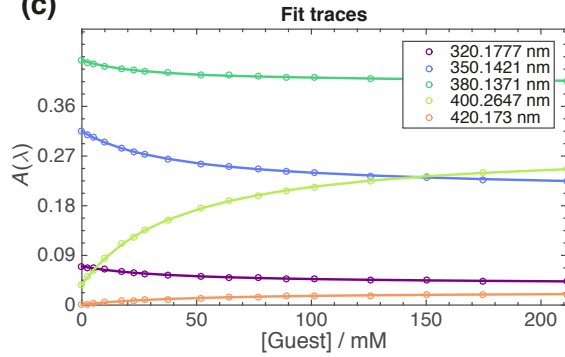
(d)



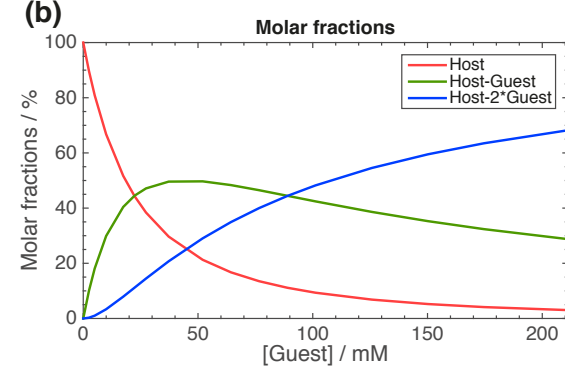
(ii) (a)



(c)



(b)



(d)

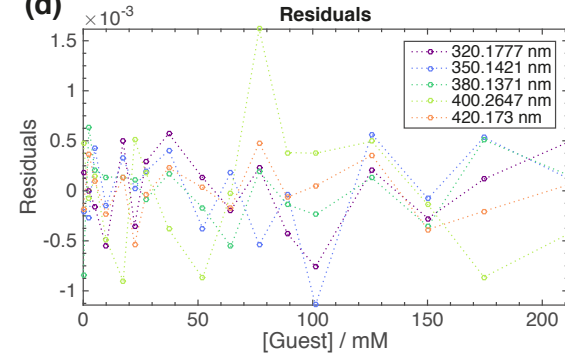


Figure S14-i: (a) Steady-state absorption spectra of C₄-dHONI ($c = 30\mu\text{M}$) upon addition of NMI in PA/BuCN mixtures, (b) best global fits, (c) residual, and (d) species spectra of H, HG and HG₂ in units of molar absorptivity ($\text{M}^{-1}\text{cm}^{-1}$). The polarity of the mixtures increases from A to E and the Δf values are indicated above each figure.

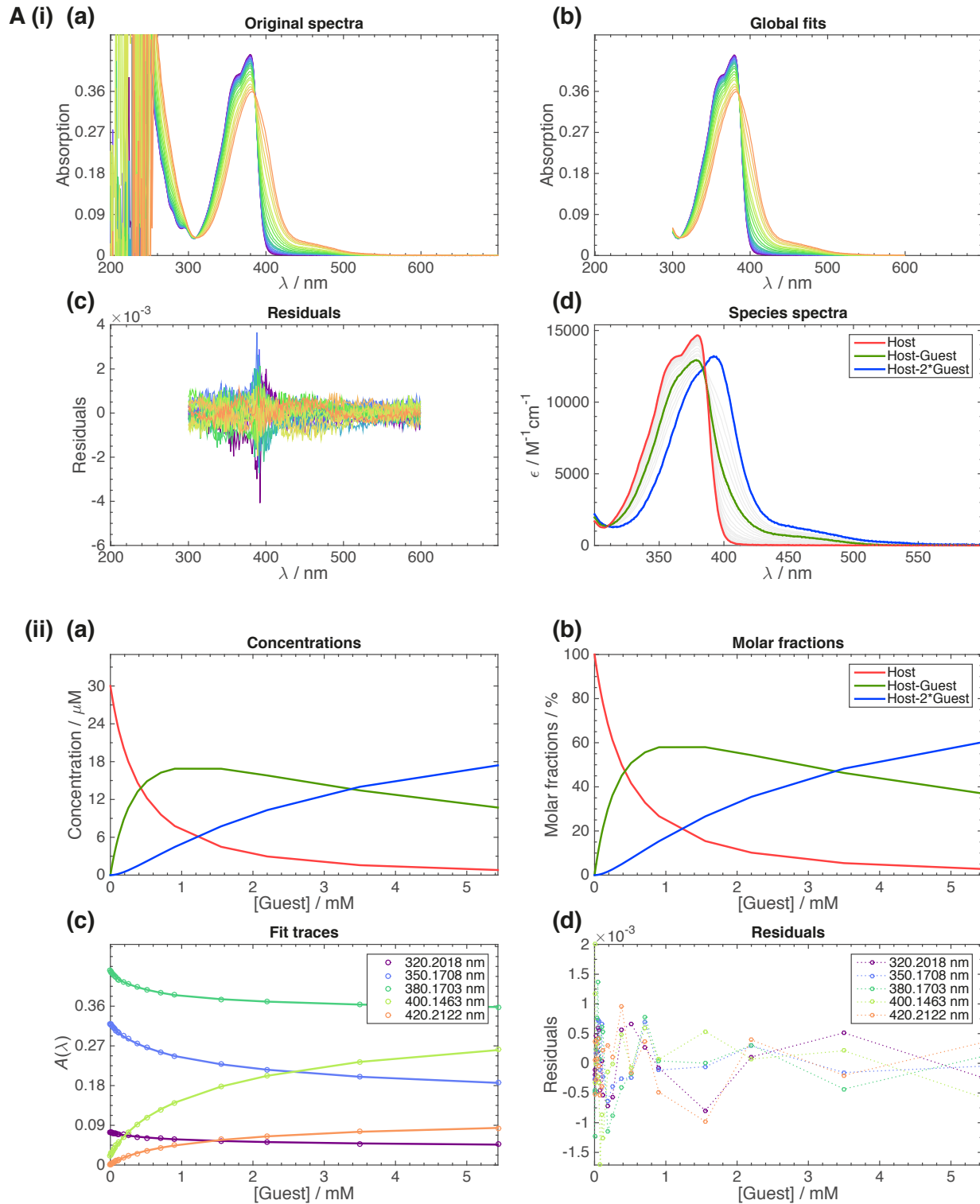
Figure S14-ii: (a) Concentrations of H, HG and HG₂, (b) corresponding molar fractions, (c) absorptions and best-fits at selected wavelengths, and (d) corresponding residuals, all as a function of the total NMI concentration in PA/BuCN mixtures.

Table S11: Ground-state association constants between a C₄-dHONI photoacid and NMI in PA/BuCN mixtures obtained from the global analysis. Non-cooperative binding ($K_1 = 4K_2$) was assumed⁷

Δf	K_1/M^{-1}	K_2/M^{-1}
0.3899	43 ± 4	11 ± 1
0.4328	43 ± 4	11 ± 1
0.4756	41 ± 4	10 ± 1
0.5187	41 ± 4	10 ± 1
0.5614	45 ± 4	11 ± 1

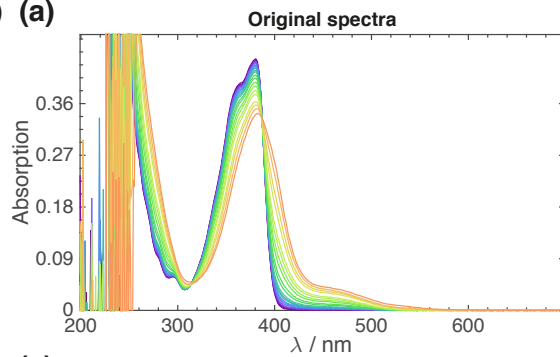
S7.2 C₄-dHONI and DBU

$$\Delta f = 0.3899$$

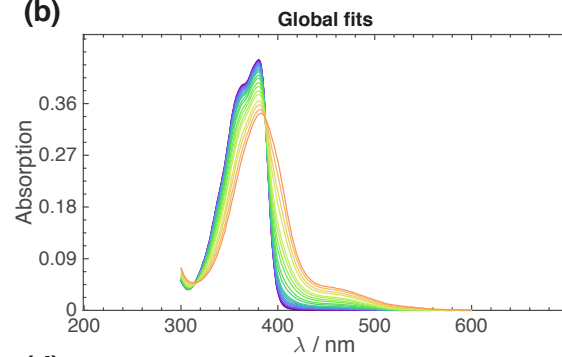


$$\Delta f = 0.4338$$

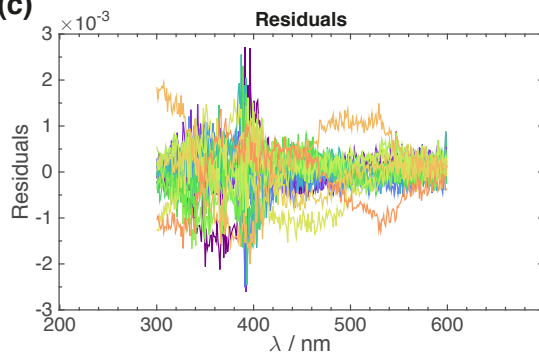
B (i) (a)



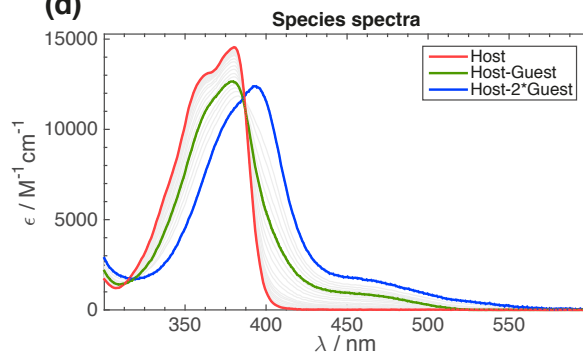
(b)



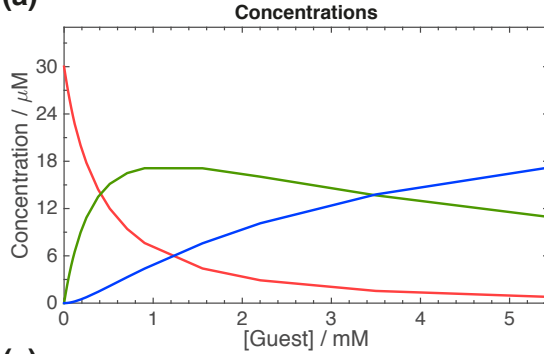
(c)



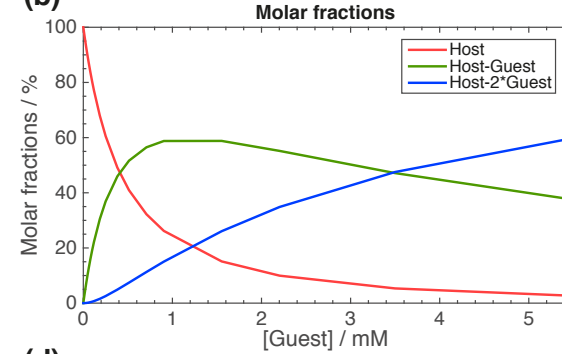
(d)



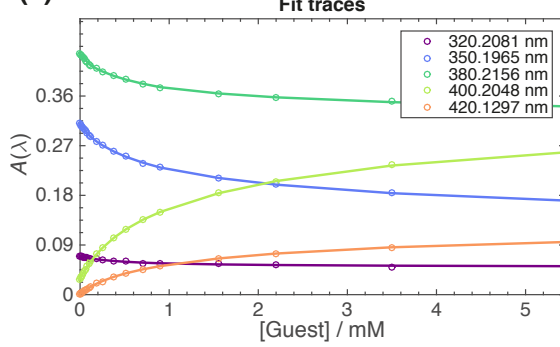
(ii) (a)



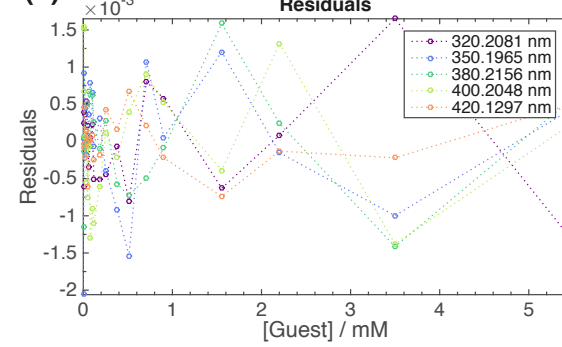
(b)



(c)

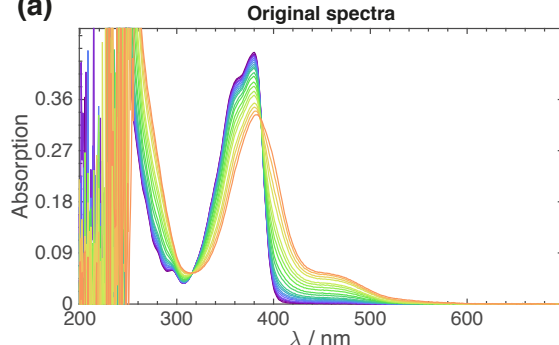


(d)

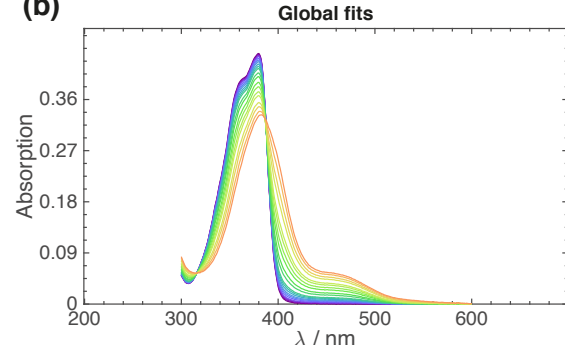


$$\Delta f = 0.4758$$

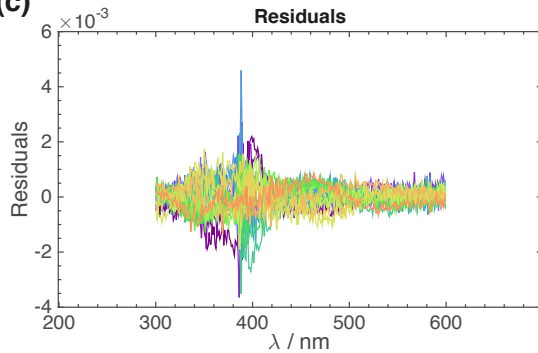
C (i) (a)



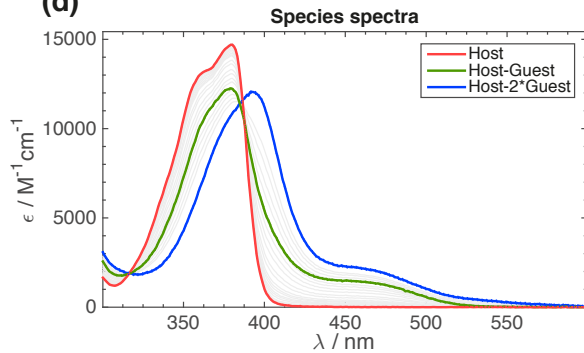
(b)



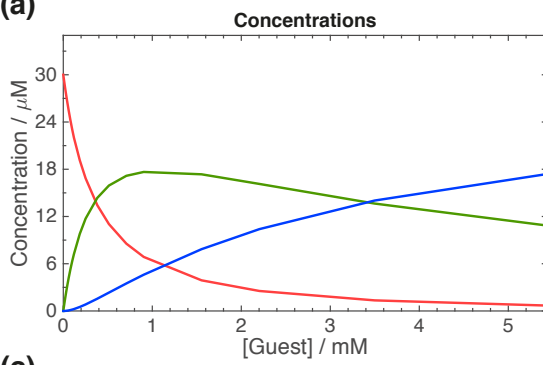
(c)



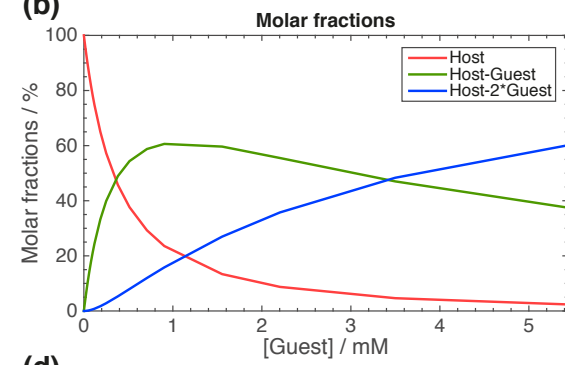
(d)



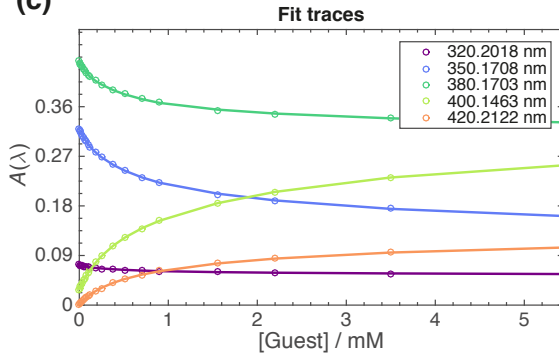
(ii) (a)



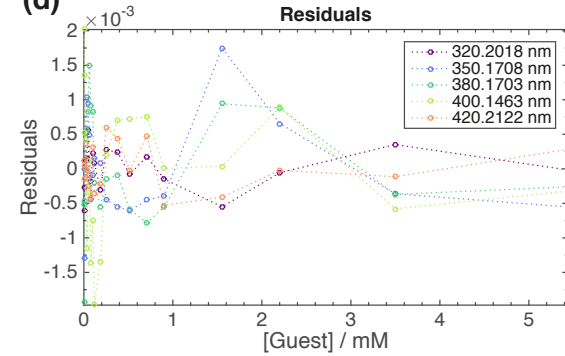
(b)



(c)

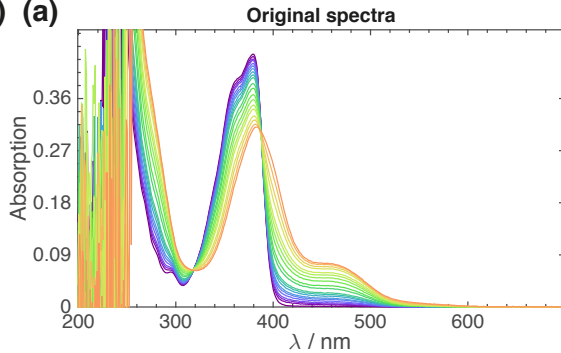


(d)

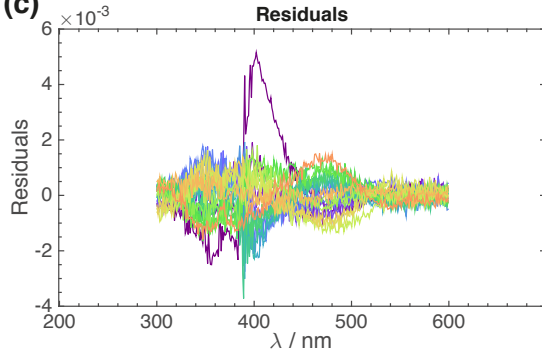


$$\Delta f = 0.5186$$

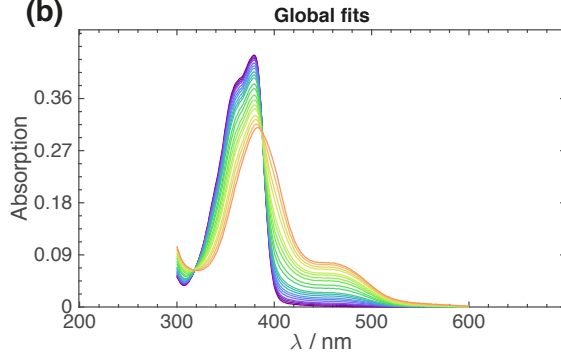
D (i) (a)



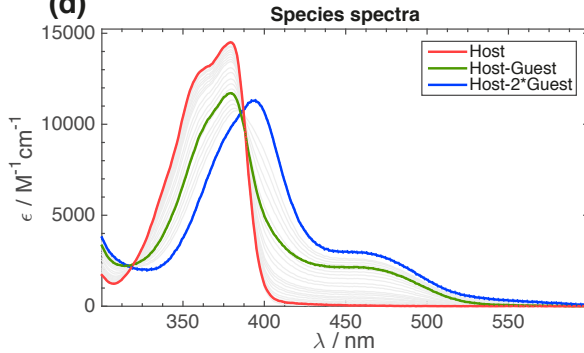
(c)



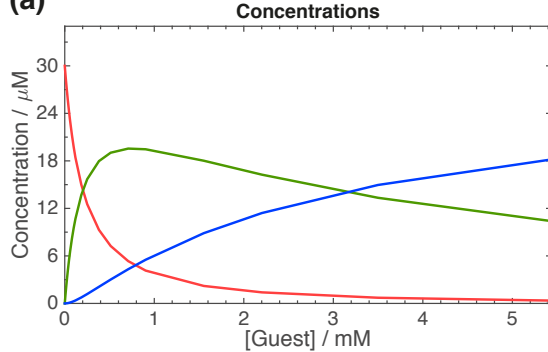
(b)



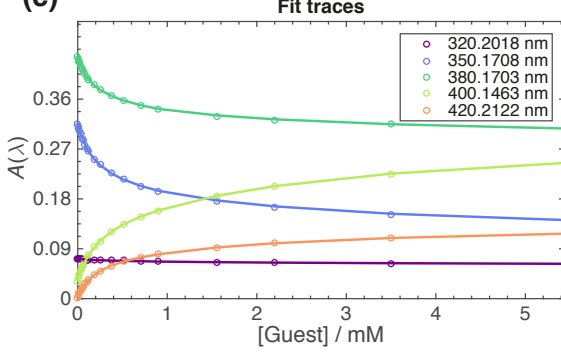
(d)



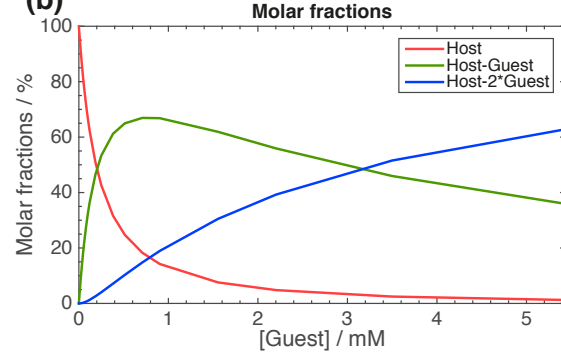
(ii) (a)



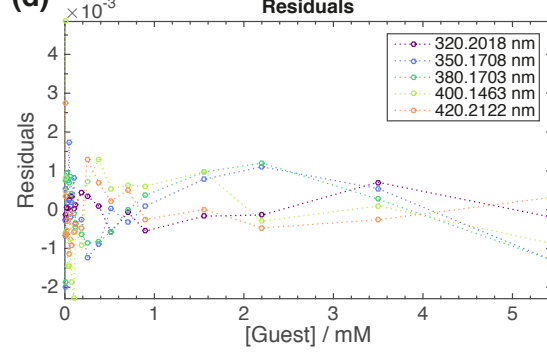
(c)



(b)

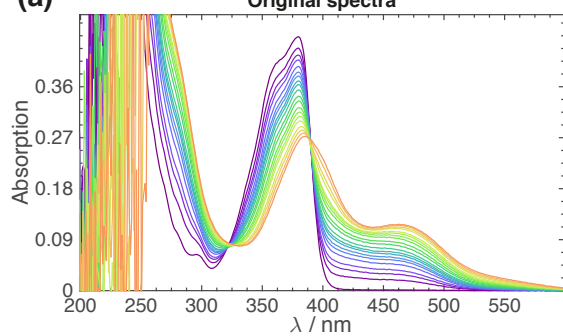


(d)

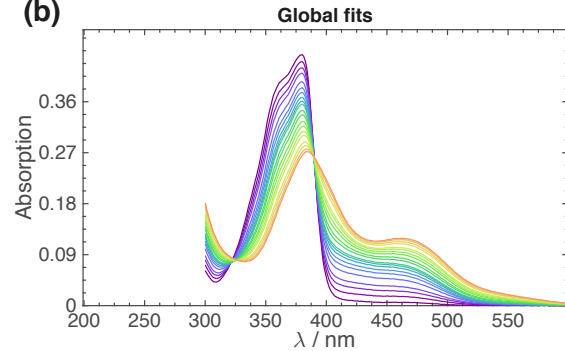


$$\Delta f = 0.5614$$

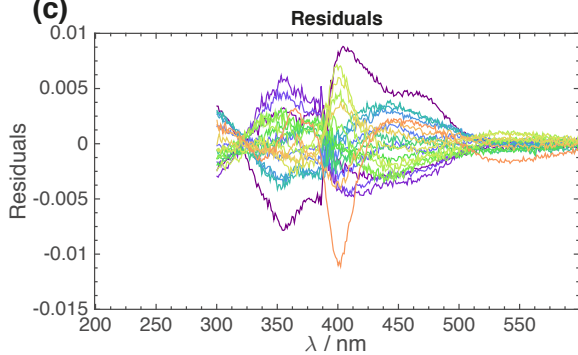
E (i) (a)



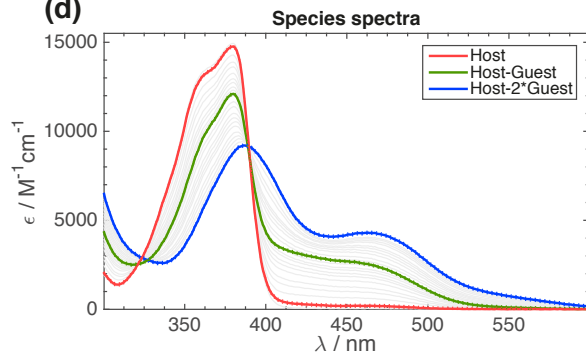
(b)



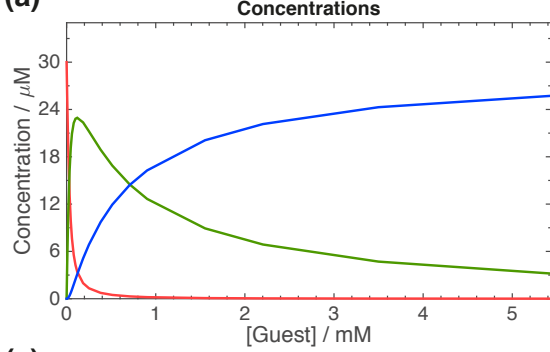
(c)



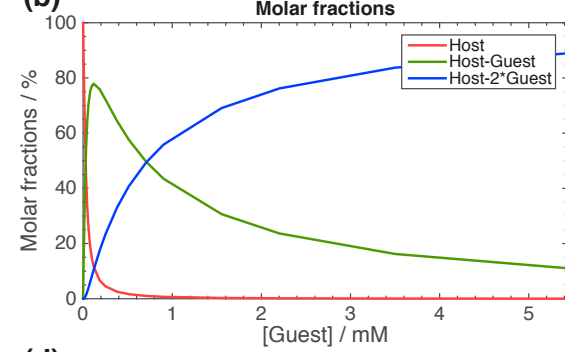
(d)



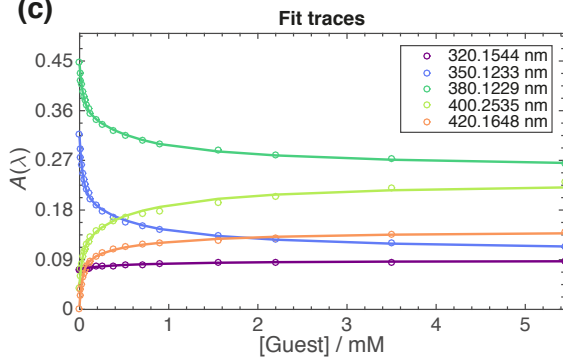
(ii) (a)



(b)



(c)



(d)

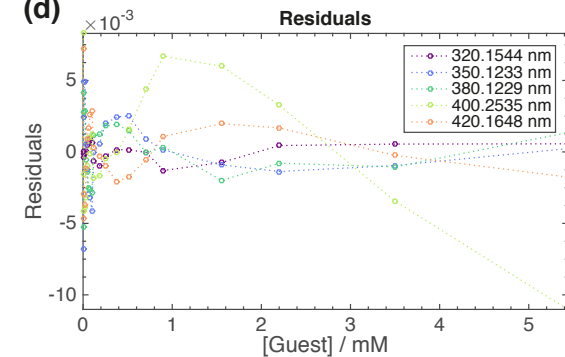


Figure S15-i: (a) Steady-state absorption spectra of C₄-dHONI ($c = 30\mu\text{M}$) upon addition of DBU in PA/BuCN mixtures, (b) best global fits, (c) residual, and (d) species spectra of H, HG and HG₂ in units of molar absorptivity ($\text{M}^{-1}\text{cm}^{-1}$). The polarity of the mixtures increases from A to E and the Δf values are indicated above each figure.

Figure S15-ii: (a) Concentrations of H, HG and HG₂, (b) corresponding molar fractions, (c) absorptions and best-fits at selected wavelengths, and (d) corresponding residuals, all as a function of the total NMI concentration in PA/BuCN mixtures.

Table S12: Ground-state deprotonation (K_1) or association (K_2) constants between a C₄-dHONI photoacid and DBU in PA/BuCN mixtures obtained from the global analysis

Δf	K_1/M^{-1}	K_2/M^{-1}
0.3899	2450 ± 90	301 ± 11
0.4338	2550 ± 80	292 ± 13
0.4758	2950 ± 60	297 ± 11
0.5186	5400 ± 70	325 ± 10
0.5614	74000 ± 3000	1500 ± 44

References

- (1) Bonilla, A.; Vassos, B. Novel Approach for Dipole Moment Laboratory Experiments. A Physical Chemistry Laboratory Experiment. *J. Chem. Educ.* **1977**, *54*, 130–131.
- (2) Marcus, Y. *The properties of solvents*, 1st ed.; Wiley: Chichester, 1998.
- (3) Angulo, G.; Grampp, G.; Rosspeintner, A. Recalling the Appropriate Representation of Electronic Spectra. *Spect. Acta Part A* **2006**, *65*, 727–731.
- (4) Fee, R. S.; Maroncelli, M. Estimating the Time-Zero Spectrum in Time-Resolved Emission Measurements of Solvation Dynamics. *Chem. Phys.* **1994**, *183*, 235–247.
- (5) Kumpulainen, T.; Rosspeintner, A.; Vauthey, E. Probe Dependence on Polar Solvation Dynamics from fs Broadband Fluorescence. *Phys. Chem. Chem. Phys.* **2017**, *19*, 8815–8825.
- (6) Hargrove, A. E.; Zhong, Z.; Sessler, J. L.; Anslyn, E. V. Algorithms for the Determination of Binding Constants and Enantiomeric Excess in Complex Host:Guest Equilibria Using Optical Measurements. *New J. Chem.* **2010**, *34*, 348–354.

- (7) Kumpulainen, T.; Bakker, B. H.; Brouwer, A. M. Complexes of a Naphthalimide Photoacid with Organic Bases, and Their Excited-State Dynamics in Polar Aprotic Organic Solvents. *Phys. Chem. Chem. Phys.* **2015**, *17*, 20715–20724.